Accepted Manuscript

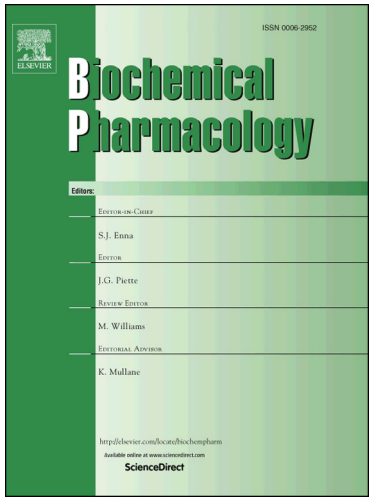

Synthesis and *in vivo* antitumor evaluation of an orally active potent phosphonamidate derivative targeting IDO1/IDO2/TDO

Xi Feng, Pei Shen, Yinuo Wang, Zhiyu Li, Jinlei Bian

PII: S0006-2952(19)30266-7
DOI: https://doi.org/10.1016/j.bcp.2019.07.011
Reference: BCP 13582

To appear in: *Biochemical Pharmacology*

Received Date: 18 May 2019
Accepted Date: 10 July 2019

Please cite this article as: X. Feng, P. Shen, Y. Wang, Z. Li, J. Bian, Synthesis and *in vivo* antitumor evaluation of an orally active potent phosphonamidate derivative targeting IDO1/IDO2/TDO, *Biochemical Pharmacology* (2019), doi: https://doi.org/10.1016/j.bcp.2019.07.011

Synthesis and *in vivo* antitumor evaluation of an orally active potent phosphonamidate derivative targeting IDO1/IDO2/TDO

Xi Feng,[a] Pei Shen,[a] Yinuo Wang,[b] Zhiyu Li*,[a] and Jinlei Bian*,[a]

[a]Jiangsu Key Laboratory of Drug Design and Optimization, Department of Medicinal Chemistry, School of Pharmacy, China Pharmaceutical University, Nanjing 210009, China

[b]Department of Biology, University of California San Diego, La Jolla, California 92093, United States

KEYWORDS: IDO1 inhibitors, Trp-Kyn, Phosphonamidate, epacadostat, NSCLC

ABSTRACT:

Targeting Trp-Kyn pathways has been identified as an attractive approach for the cancer immunotherapies. In this study, a novel phosphonamidate containing compound was designed, synthesized and evaluated for its inhibitory activity against key dioxygenases in Trp-Kyn pathway, including IDO1, IDO2 and TDO. This compound showed potent IDO1 inhibitory activity with an IC_{50} value of 94 nM in an enzymatic assay and 12.6 nM in HeLa cells. In addition, this compound showed promising IDO2 inhibition and TDO inhibition with IC_{50} values of 310 nM and 2.6 μM, respectively, in enzyme assay. Based on the promising enzyme inhibitory activity toward IDO/TDO, compound **F04** was evaluated of its antitumor effects in two tumor models. Further evaluation of mechanism demonstrated compound **F04** with the remarkable capacity of reducing kynurenine level in plasma/TME and restoring anti-tumor immune response. **F04** could be further developed as a potential immunotherapeutic agent combined with immune checkpoint inhibitors or chemotherapeutic drugs for cancer treatment.

1. Introduction

L-tryptophan (L-Trp) is the least abundant of the essential amino acids but is essential for maintaining several cellular functions. L-Trp could be metabolized through four mechanisms, including decarboxylation to tryptamine, protein synthesis, the serotonin pathway and the kynurenine pathway (KP) [1,2]. Among them, the KP is responsible for the metabolism of approximately 95% of all mammalian dietary tryptophan [3].

The heme-containing enzymes, indoleamine 2,3-dioxygenase 1 (IDO1), indoleamine 2,3-dioxygenase 2 (IDO2) and tryptophan 2,3-dioxygenase (TDO) are cytosolic heme-containing enzymes that catalyze the initial and rate-limiting step of the L-tryptophan (L-Trp) catabolism through KP [4,5]. These heme-containing enzymes negatively modify cellular immune response by a molecular mechanism of depleting local tryptophan storages and producing immunological active KP metabolites [6,7]. Among the three enzymes, IDO1 has been studied for over 25 years which has been proved to be overexpressed in majority cancers [5]. High IDO1 expression is usually associated with poor prognosis in a variety of cancer types [8,9]. Increasing evidence revealed that IDO1 contribute to the arising of resistance against immune checkpoint blockade therapies [10,11], and correspondingly, the combination of checkpoint inhibitors with IDO1 inhibition offers an advanced strategy in cancer immunotherapy and showed efficiency in clinical trials [12–14]. Thus, targeting the IDO1 pathway is an attractive approach for cancer immunotherapy [15]. Indoleamine 2,3-dioxygenase 2 (IDO2), comparing to IDO1, is known as the other isoform of IDO which shares 43% sequence identity and functions with distinct biochemical features [16,17]. Although been less thoroughly studied and restrictively expressed in both normal or tumor tissues, IDO2 has been found to be a contributor to IDO1-mediated immune tolerance [18]. As for intrahepatic enzyme tryptophan 2,3-dioxygenase (TDO), it is strongly expressed in hepatocarcinoma and catalyzes the same reaction as IDO in rate-limiting manner and overexpressed in some tumors as a mean of immune escape [19].

Recently, great attention has been paid on IDO1 inhibitors development both in academia and pharmaceutical industry. Especially for the recent negative outcome of an ECHO-301 phase 3 trial with selective IDO1 inhibitor epacadostat (INCB24360), many researchers were frustrated with the result. However, the failure may relate to inapplicable pharmacodynamical index or mismatched drug combination strategy [20]. There are still 35 clinical trials in the active state for several IDO1 inhibitors, indicated that IDO1 related therapy will continue to be an exciting area [21]. In addition, the failure of ECHO-301 phase 3 trial may due to the highly selective toward IDO1 than TDO and IDO2 [20]. Thus, developing combo or pan IDO1/IDO2/TDO inhibitors may broaden the impact in cancer treatment and overcome the deficiency in clinical trials of IDO1 selective inhibitors [22,23].

Our group has been focused on the discovery of potent IDO1 inhibitors for several years. In this work, we would report a novel IDO1/IDO2/TDO inhibitor **F04** containing a phosphonamidate subunit. Our objective was to synthesize potent inhibitor targeting key dioxygenases in Trp-Kyn pathway. Interestingly, the compound showed potent IDO1 inhibitory activity as well as moderate IDO2/TDO inhibitory activity by involving in the rarely applied functional group. In addition, **F04** showed an improved drug-like property than clinical candidate epacadostat. The further *in vivo* investigation demonstrated that **F04** could remarkably suppress tumor progression both in immunocompetent C57BL6 mice and lung metastasis of Lewis cells model, which was more potent than epacadostat. Furthermore, the mechanism study showed that tumors from **F04**-treated mice at 60 mg/kg exhibited a markedly reduced Kyn/Trp ratio comparing to epacadostat. Therefore, **F04** was deserved further optimization with the aim to obtain antitumor agents through targeting Trp-Kyn pathway.

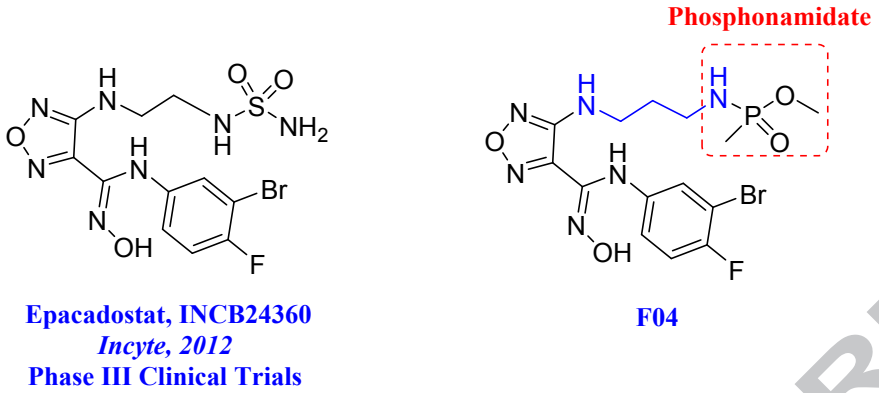

Fig. 1. Structure of candidate epacadostat and the structure of compound **F04** contained in the rectangle with broken line was modified from epacadostat with the phosphonamidate moiety.

2. Materials and methods

2.1. General experimental methods

Unless otherwise noted, all reagents were obtained from commercial suppliers and used without further purification. NMR spectra were measured on a 300 MHz Bruker unit (300 MHz for ^{1}H NMR, 75 MHz for ^{13}C NMR, 121 MHz for ^{31}P NMR) using $CDCl_3$ or DMSO-d_6 as the solvent at room temperature. MS spectra were recorded on a LC/MSD TOF HR-MS Spectrum. Melting points were determined on a Mel-TEMP II melting point apparatus without correction.

*2.1.1. Synthesis of phosphonchloride **10***

Phosphonchloride **10** was prepared according to the method described by McAnoy *et al* [24]. Dimethyl methylphosphonate (20 mmol) was treated with oxalyl chloride (30 mmol, 1.5 equiv) and additional drops of *N,N*-dimethylformamide were added as catalyst. The desired product was obtained as garnet liquid (1.2 g, 49%) and used for the next step without further purification.

*2.1.2. Synthesis of 4-amino-N-hydroxy-1,2,5-oxadiazole-3-carboximidoyl chloride (**5**)*

Intermediate **5** was prepared strictly according to literature procedure described by Tao *et al* [25]. (a) Commercially available malononitrile (9.9 g, 150 mmol), sodium nitrite (20.7 g, 300 mmol), hydroxylamine hydrochloride (23 g, 340 mmol) were employed and 4-amino-*N*′-hydroxy-1,2,5-oxadiazole-3-carboximidamide **2** was generated in a one-pot reaction as while solid (14.9 g, 68%). ^{1}H NMR (300 MHz, DMSO-d_6): δ = 10.46 (s, 1H), 6.24 (s, 2H), 6.02 (s, 2H) ppm. (b) Next, intermidiate **2** (4.2 g, 29.5 mmol) was mixed with sodium chloride (5.2 g, 88.5 mmol), water (59 mL), acetic acid (29 mL) and 6 N hydrochloric acid solution (14.6 mL, 88.5 mmol) then sodium nitride (2.0 g, 29 mmol) was added to the resulting suspension by drops under 0 °C. The target compound **3** was obtained as an off-white solid (2.5 g, 53%). ^{1}H NMR (300 MHz, DMSO-d_6): δ = 13.39 (s, 1H), 6.29 (s, 2H). (c) 4-Amino-*N*-hydroxy-1,2,5-oxadiazole-3-carboximidoyl chloride **3** (3.24 g, 20 mmol) was mixed with water (70 mL) and 3-bromo-4-fluoroaniline (4.18 g, 22 mol, 1.1 equiv). At 60 °C, a solution of sodium bicarbonate (3.36 g, 40 mmol, 2 equiv) in water (15 mL) was added to the mixture by drops then resulting mixture was heated to reflux. After purification, compound **4** was obtained as a white solid (5.75 g, 91%). ^{1}H NMR (300 MHz, DMSO-d_6): δ = 11.46 (s, 1H), 8.89 (s, 1H), 6.99 (t, J = 8.8 Hz, 1H), 6.81 (dd, J_1 = 6.0 Hz, J_2 = 2.7 Hz, 1H), 6.56–6.51 (m, 1H), 6.28 (s, 2H) ppm. (d) Last, **4** (5.0 g, 15.8 mmol) was treated with *N*,*N*′-carbonyldiimidazole (5.12 g, 31.6 mmol, 2 equiv) at room temperature to give 3-(4-amino-1,2,5-oxadiazol-3-yl)-4-(3-bromo-4-fluorophenyl)-1,2,4-oxadiazol-5(4*H*)-one **5** as white solid (4.80 g, 89%). ^{1}H NMR (300 MHz, DMSO-d_6): δ = 8.10 (dd, J_1 = 6.2 Hz, J_2 = 2.4 Hz, 1H), 7.74–7.69 (m,1H), 7.61 (t, J = 8.6 Hz, 1H), 6.60 (s, 2H) ppm.

*2.1.3. Synthesis of 4-(3-bromo-4-fluorophenyl)-3-(4-nitro-1,2,5-oxadiazol-3-yl)-1,2,4-oxadiazol-5(4H)-one (**6**)*

5 (4.5 g, 13.1 mmol) was mixed with 30% hydrogen peroxide (30 mL) and trifluoroacetic acid (90 mL) then the resulting mixture was stirred at 45 °C overnight. After transformation, 4-(3-bromo-4-fluorophenyl)-3-(4-nitro-1,2,5-oxadiazol-3-yl)-1,2,4-oxadiazol-5(4*H*)-one **6** was obtained as a yellow solid (2.19 g, 45%). ^{1}H NMR (300 MHz, DMSO-d_6): δ = 8.06 (dd, J_1 = 6.0 Hz, J_2 = 2.3 Hz, 1H), 7.69–7.64 (m, 1H), 7.60 (t, J = 8.6 Hz, 1H) ppm.

*2.1.4. Synthesis of 3-{4-[(3-aminopropyl)amino]-1,2,5-oxadiazol-3-yl}-4-(3-bromo-4-fluorophenyl)-1,2,4-oxadiazol-5(4H)-one hydrochloride (**8**).*

6 (1.86 g, 5 mmol) and *N*-Boc-1,3-propanediamine (1.74 g, 10 mmol, 2equiv) was dissolved in tetrahydrofuran (50 mL) followed by the addition of aqueous 2N NaOH (5 mL, 2 equiv) and the reaction mixture was stirred at room temperature for 2 h. After purification by column chromatography on silica gel, tert-butyl [2-({4-[4-(3-bromo-4-fluorophenyl)-5-oxo-4,5-dihydro-1,2,4-oxadiazol-3-yl]-1,2,5-oxadiazol-3-yl}amino)propyl]carbamate **7** was obtained as a pale-yellow solid (1.37 g, 55%). ^{1}H NMR (300 MHz, DMSO-d_6): δ = 8.09–8.07 (m, 1H), 7.72–7.70 (m, 1H), 7.60 (t, J = 8.4 Hz, 1H), 6.93 (s, 1H), 6.51 (s, 1H), 3.31 (s, 2H), 3.08 (s, 2H), 1.85 (s, 2H), 1.37 (s, 9H) ppm. Next, **7** (1.2 g, 2.40 mmol) was treated with hydrogen chloride (10 mL, 4.0 M in ethyl acetate) at room temperature to afford 3-{4-[(3-aminopropyl)amino]-1,2,5-oxadiazol-3-yl}-4-(3-bromo-4-fluorophenyl)-1,2,4-oxadiazol-5(4*H*)-one hydrochloride **8** as an off-white solid (0.93 g, 89%). ^{1}H NMR (300 MHz, DMSO-d_6): δ = 8.12 (dd, J_1 = 6.0 Hz, J_2 = 2.2 Hz, 1H), 8.04 (sbr, 3H), 7.77–7.72 (m, 1H), 7.61 (t, J = 8.6 Hz, 1H), 6.75 (s, 1H), 3.35–3.33 (m, 2H), 2.83–2.81 (m, 2H), 1.91–1.87 (m, 2H) ppm.

*2.1.5. Synthesis of methyl N-[3-({4-[N-(3-bromo-4-fluorophenyl)-N'-hydroxycarbamimidoyl]-1,2,5-oxadiazol-3-yl}amino)propyl]-P-methylphosphonamidate (**F04**)*

Hydrochloride **8** (0.44 g, 1 mmol) was treated with phosphonochloridate **10** (0.38 g, 3 mmol, 3 equiv) at 0 °C in dry dichloromethane (30 mL) then triethylamine (0.30g, 3 mmol, 3 equiv) was added. The reaction mixture was allowed warm to ambient temperature and stirred for 1 h. **11** was then obtained as a pale-yellow solid without further purification and used for the next step immediately. Crude **11** was dissolved in tetrahydrofuran (20 mL) and treated with 2 N NaOH (4 mL). Deprotection was performed at room temperature and target compound **F04** was ultimately obtained after purification by column chromatography on silica gel as a pale-yellow solid (0.17 g, 37% for two steps). mp = 103–105 °C. ^{31}P NMR (121 MHz, DMSO-d_6): δ = 34.6 ppm. ^{1}H NMR (300 MHz, DMSO-d_6): δ = 11.58 (s, 1H), 8.91 (s, 1H), 7.19 (t, J = 8.7 Hz, 1H), 7.11 (d, J = 3.3 Hz, 1H), 6.78–6.77 (m, 1H), 6.39 (s, 1H), 4.78–4.73 (m, 1H), 3.35 (d, J = 11.1 Hz, 3H), 3.27–3.26 (d, J = 5.7 Hz, 2H), 2.86–2.83 (m, 2H), 1.71–1.69 (m, 2H), 1.35 (d, J = 16.3 Hz, 3H) ppm. ^{13}C NMR (75 MHz, DMSO-d_6): δ = 155.5, 152.1, 139.9, 139.1, 137.9, 124.7, 121.4 (J = 6.9 Hz), 116.0 (J = 23.2 Hz), 107.1 (J = 22.0 Hz), 49.7 (J = 6.3 Hz), 41.7, 37.7, 30.1 (J = 5.6 Hz), 12.0 (J = 129.2 Hz) ppm. HRMS (ESI$^+$): cacld for $C_{14}H_{19}BrFN_6O_4P$ $(M + H)^+$, 465.0446; found, 465.0444.

2.2. Materials

2.2.1. Cell culture and reagents.

Lewis lung carcinoma cells was purchased from Cell Bank of Shanghai Institute of Biochemistry and Cell Biology, Chinese Academy of Sciences (Shanghai, China) and grown in DMEM (Gibco, Grand Island, NY) supplemented with 10% heat-inactivated fetal bovine serum (FBS) (Gibco, Grand

Island, NY) and 1% penicillin/streptomycin (all from Invitrogen). Ki67 was obtained from R&D System (MN, USA). Epacadostat was purchased from CSNpharm (CSN13892, USA).

2.2.2. Mice.

Eight-week-old male C57BL/6 mice, weighing 18–22 g, were supplied by Model Animal Genetics Research Center of Nanjing University (Nanjing, China). Mice were maintained under standard specific-pathogen-free (SPF) conditions (23 ± 2°C and 12-h light:dark cycle with a relative humidity of 45 ± 10%) and all research involving animals strictly complied with protocols approved by the Animal Welfare and Ethics Committee (AWEC, China Pharmaceutical University). In the tumor transplanting experiments, the mice were inoculated subcutaneously with 6×10^5 Lewis tumor cells. Mice bearing Lewis tumor were randomly divided into 5 groups. **F04** at doses of 15 mg/kg, 30 mg/kg and 60 mg/kg or epacadostat at 60 mg/kg, dissolved in 0.5% carboxymethylcellulose sodium (CMC-Na), were administered i.g. daily until termination of the experiment, and in the control group, the same volume of CMC-Na was gavaged as vehicle control. Tumor volume was measured using a digital vernier caliper every 3 days post tumor inoculation using the formula $V = \pi \times \text{length} \times \text{width}^2/6$. Tumors were harvested on day 30 for further use. In the Tumor metastasis experiments, Lewis tumor cells were prepared as a suspension of 10^6 cells in 150 μL saline and injected into the lateral tail vein using a 29-gauge needle under sterile conditions. Mice were weighed every 3 days and lung metastasis was determined by counting the total number of metastatic nodules in each lung.

2.3. Cell-based IDO1 activity assay.

Performed according to the literature protocol [26]. HeLa cells were seeded in 96-well culture plates at a density of 5×10^4 per well. The following day, after growth media was aspirated, human hIFN-γ (20 ng/well, Sigma-Aldrich SRP3058-100UG), L-Trp (15 μg/mL) and serial dilutions of test

compounds were added to the 96-well plates (200 μL final volume per well). After incubation at 37 °C for 48 h, 140 μL of the supernatant was transferred to a new 96-well plate and mixed with 10 μL of 6.1 N trichloroacetic acid for 30 min at 50 °C to hydrolyze *N*-formlylkynurenine. Then the mixture was cooled at 0 °C and centrifuged at 4000 rpm for 20 min. Subsequently, another 100 μL of the supernatant was taken and added to a new 96-well plate and 100 μL of 2% (w/v) *p*-dimethylaminobenzaldehyde (*p*-DMAB, Ehrlich's reagent) in acetic acid was added. The amount of generated kynurenine was determined by the absorbance at 480 nm. Graphs of inhibition curves with IC_{50} values were generated using Prism GraphPad. Epacadostat was purchased from CSNpharm (Cat. CSN13892, USA).

2.4. hIDO1, hIDO2 and hTDO enzymatic inhibition assay.

Human IDO1 with an *N*-terminal His Tag was expressed in *E. coli* and purified by Ni-NTA Agarose (Invitrogen R90101). The assay was performed by UV absorption using hIDO1 and L-Trp as substrates. The UV absorption signal at 321 nm is correlated with the amount of generated *N*-formylkynurenine and determined by EnSpire. The initial reaction rates were recorded by continuously following the absorbance increase at 321 nm as a consequence of the formation of *N*-formylkynurenine. The percent inhibition at individual concentrations was calculated by the slopes and the IC_{50} values were generated using nonlinear regression (Prism GraphPad). hIDO2 and hTDO were purchased from commercial source (BPS Bioscience, Cat. #71194-2 and #71195) and the inhibition assay was detailed described in ref 27.

2.5. Caco-2 assay.

Permeability was studied with the Caco-2 monolayer cultured for 4-5 days (>500 cm^2 in each well) and added the HBSS buffer containing 10 mM HEPES and test compounds. The test sample was taken

from both apical and basolateral chambers at 0 and 90 min after incubation at 37 °C and analyzed by LC-MS/MS. The calculation formula of efflux ratio is P_{app} (B→A)/ P_{app} (A→B).

2.6. Histological analyses

For histology, lung tissues were fixed in 4% paraformaldehyde (PFA) and paraffin-embedded sectioned were deparaffined and rehydrated, followed by hematoxylin and eosin (H&E) staining.

2.7. FACS analysis

Transplanted tumors were dissected into pieces and digested in 1 × HBSS buffer including 2% FBS, 1 mg/ml collagenase I (Sigma-Aldrich) and 0.5 mg/ml dispase (Invitrogen), followed by further digestion in 10 μg/mL DNase (Invitrogen) for 45 min, and in 0.64% ammonium chloride (STEMCELL Technologies) for 5 min at 37 ℃. Cells were filtered through a 70-μm cell strainer (BD Biosciences), and resuspended in 1 × HBSS buffer containing 2% FBS, followed by a gradient centrifugation in Ficoll-Pague (Sigma-Aldrich). Purified lymphocytes were stained using a fixation and permeabilization kit (eBioscience) and analyzed by FACS analysis to detect expressions of CD45, CD4, CD8, Foxp3 (Biolegend) and Ki67 (Cell Signaling Technology).

2.8. Tryptophan/kynurenine measurement

In IDO1 enzyme activity measurement, blood and Tumors from vehicle-, **F04**- and epacadostat-treated mice were collected. Tumors were homogenized in 3 volumes of saline with 0.1% formic acid. Following protein-precipitation extraction with methanol, plasmas and tumor homogenates were collected and 20 μL of the supernatants were subjected to LC/MS/MS analysis. Aqueous standards were prepared for adjustment of endogenous tryptophan and kynurenine levels.

2.9. Immunofluorescence

Immunofluorescence was performed on paraffin-embedded colonic tissue sections. The sections were deparaffinized, rehydrated and washed in 1% PBS-Tween. Then they were treated with 3% hydrogen peroxide, blocked with 10% goat serum and incubated with Ki67 and CD8 primary antibody (Abcam) overnight at 4 °C, followed by incubation with goat anti-rat Alexa 488, goat anti-rabbit Alexa 594 secondary antibodies (all from Invitrogen) for 1 h at room temperature. The slides were stained with DAPI. Images were acquired by confocal laser-scanning microscope (Olympus, Lake Success, NY). Settings for image acquisition were identical for control and experimental tissues. Immunoblots with the tissue of interest were used to determine whether the primary antibody can bind to a single protein of the correct molecular weight.

2.10. Statistical analysis

Most results are presented as the mean ± SD. Data sets consisting of more than 2 groups were analyzed by analysis of variance (ANOVA) with Tukey-Kramer HSD post test for multiple comparisons if significance was determined. For data not conforming to a normal distribution, Kruskal-Wallis test was used for multiple comparisons. P value that was less than 0.05 was considered statistically significant for all data sets. All statistical analysis was performed using GraphPad Prism software.

2.11. Water solubility assay

Compound (1 mg) was added to 1 mL of water and the result mixture was shaked at 25 °C for 30 h. The suspensions were filtered and determined by HPLC in 254 nm. Quantification of each compound was calibrated by comparison with linear standard curve established from standard solution in methanol. Determination was performed in duplicate.

3. Results

3.1. Chemistry

The synthetic pathway for phosphonamidates **F04** is depicted in Fig. 2. Intermediate **2** was synthesized in a one-pot reaction from commercially available malononitrile (**1**, Fig. 2) in a yield of 68%. **2** was then treated with sodium nitrite in water to afford **3** in 53% yield. **4** was obtained through a nucleophilic substitution reaction with substituted aniline and subsequently transformed to amino-furazan **5** with the addition of *N,N′*-carbonyldiimidazole in adorable yields of 91% and 89% respectively. Next, the amino group of **5** was oxidized by hydrogen peroxide in trifluoroacetic acid to afford nitro-furazan **6** in a moderate yield of 45%. Subsequently, **7** was obtained in good yield by treating **6** with *N*-Boc-1,3-propanediamine and then deprotected in hydrogen chloride to give **8** as a hydrochloride salt. Amidation of **8** with phosphonchloride **10** generated intermediate **11** and an additional deprotection was performed to give the target compound **F04** in a yield of 37%.

*3.2. **F04** showed good activity toward IDO1, IDO2 and TDO*

F04 was first evaluated on IDO1, IDO2 and TDO inhibition activity. The IDO1 inhibitory activity was determined in IDO1 HeLa assay and IDO1 enzyme assay while IDO2/TDO inhibitory activity were determined in enzyme assay. Clinical candidate epacadostat was selected as control. As shown in Fig. 3, **F04** was first evaluated for its IDO1 inhibitory activities in IDO1 HeLa assay and IDO1 enzyme assay. It was found that **F04** showed equal potency in HeLa assay with IC_{50} of 12.6 nM and enzyme IC_{50} of 94.5 nM comparing to the control epacadostat (HeLa IDO1 IC_{50} = 10.1 nM, hIDO1 IC_{50} = 72.2 nM). In addition, compound **F04** displayed improved potency against IDO2 (IC_{50} = 310 nM) comparing to positive control epacadostat (IC_{50} = 0.71 μM) and moderate TDO enzyme IC_{50} of 2.6 μM, in spite of the evident diversity between two protein structures of IDO1 and TDO. It should

be noted that the control epacadostat showed low inhibitory activity toward TDO with IC_{50} > 10 μM. In general, the new compound **F04** showed pan inhibition of IDO1/IDO2/TDO comparing to the clinical candidate epacadostat which confirmed as selective IDO1 inhibitors [4]. This characteristic of compound **F04** may plumb the full potential of blunting Trp catabolism which may be benefit for the therapy in clinical.

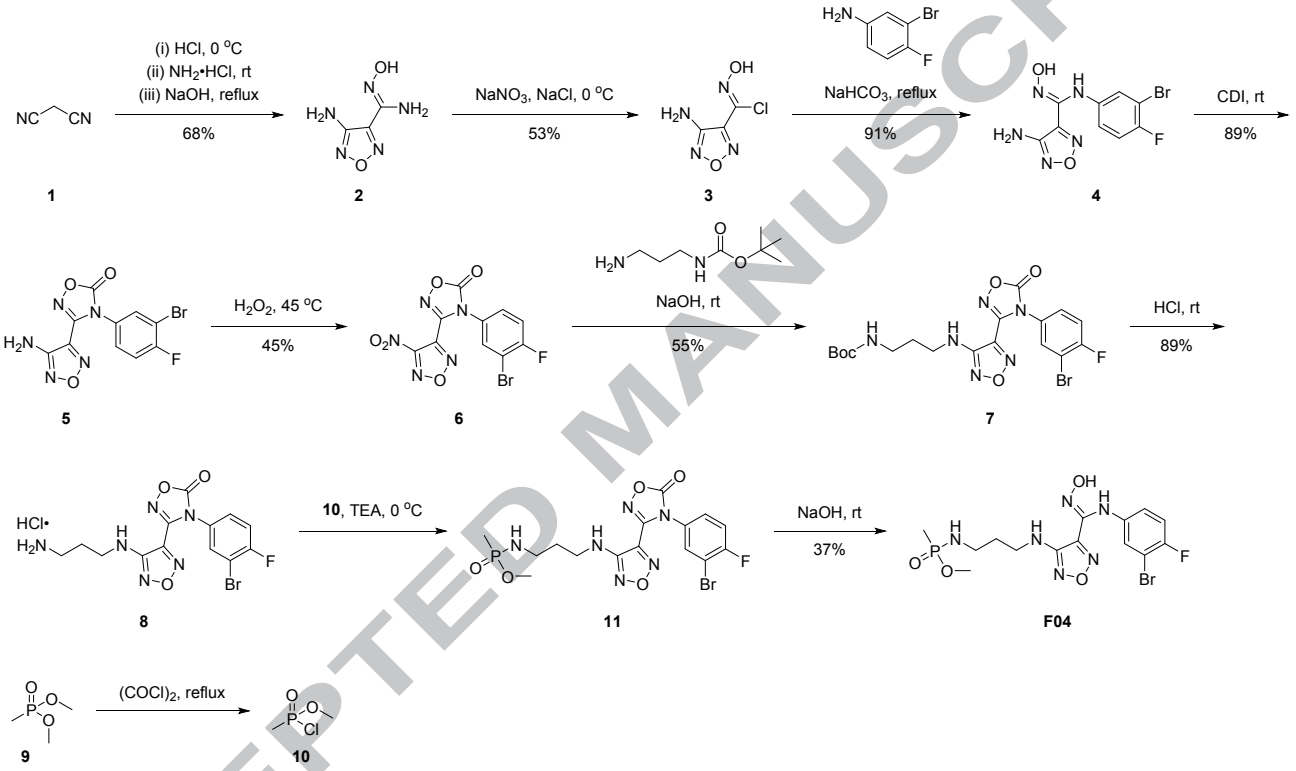

Fig. 2. Synthetic scheme for **F04**

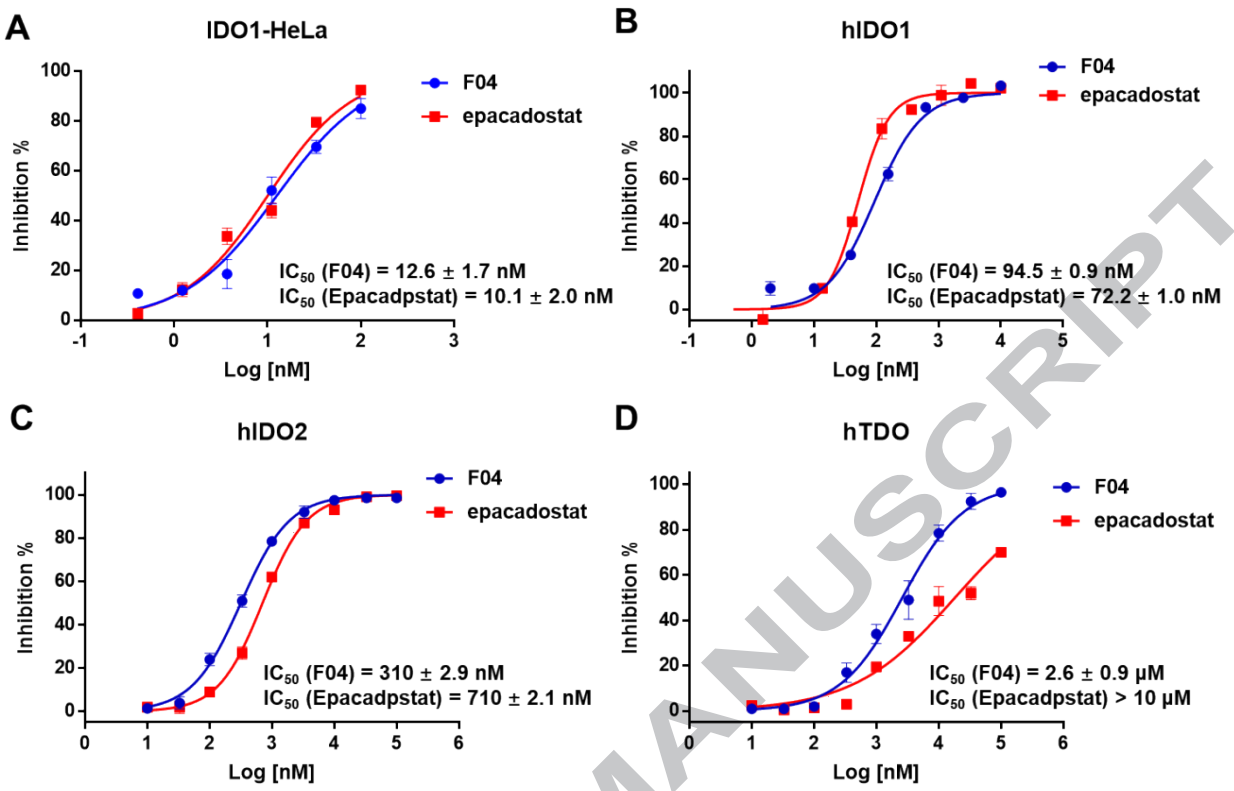

Fig. 3. The inhibitory curves of compound **F04** and epacadostat targeting IDO1-HeLa (A); hIDO1 (B); hIDO2 (C) and TDO (D).

*3.3. Physicochemical properties of compound **F04***

In an effort to identify potential drug-like compounds prior to the time-consuming and costly development to optimize derivatives that may ultimately fail in *in vivo* experiments, then **F04** was employed to determine its physicochemical properties (Table 1). Introducing phosphonamidate group comparing to sulfamide, **F04** exhibited lower polarity with the support of reduced polar surface area (PSA < 140 Å^2, **F04** PSA = 129 Å^2) [28] and favorable cLogP. Following this, moderated permeabilities were confirmed as expected in Caco-2 assay ($P_{app\ A\text{-}B}$ = 2.0 × 10^{-6} cm/s) with no significant efflux (efflux ratio = 1.10). In addition, **F04** was characterized by improved water solubility values (S = 0.18 mg/mL) than compound **1** (S = 0.13 mg/mL). Further, this compound **F04** was in line with Lipinski's rule-of-five (HBD < 5, HBA < 10, MW < 500) [29]. Subsequently, ligand efficiency (LE) and lipophilic ligand efficiency (LLE) were calculated based on cell IC_{50} which were

instructive in drug candidate development [30] and result revealed that **F04** displayed ideal values (LE = 0.40, LLE = 5.3). Till now, findings aforementioned demonstrate that **F04** displays good potential as an oral drug.

Table 1

Calculated property of phonphonamidate derivative **F04**.

Cpds	HeLa IDO1 IC_{50} (nM)	IDO1 IC_{50} (nM)	Caco-2[a] (cm/s)	S[b] (mg/mL)	PSA[c]	cLogP	HBD[d]	HBA[d]	MW	LE[e]	LLE[e]
F04	12.6	94	2.0 (1.10)	0.18	129	2.5	4	10	465	0.40	5.3
epacadostat	10.0	72	3.1 (1.09)	0.13	163	1.5	6	11	438	0.44	6.5

[a]Caco-2 values: $P_{app} \times (10)^{-6}$ cm/s with efflux ratio in bracket. [b]Aqueous solubility and each value was represented as a mean from two trials. [c]PSA in $Å^2$ (calculated using ChemBioDraw Ultra 13.0). [d]Hydrogen bond donor and acceptor. [e]Ligand efficiency (LE) and lipophilic ligand efficiency (LLE) calculated using HeLa pIC_{50}.

3.4. Molecular modeling.

Utilizing the crystal structure of IDO1 (PDB id: 5WN8), computational study was performed to elucidate the possible binding mode of IDO1 with the representative compound **F04** (Fig. 4A). The compound oriented with the similar pose with the native ligand epacadostat (Fig. 4B) [31]. The phosphonamidate group bound in pocket B and formed two strong hydrogen bonds with Arg231. In addition, the NH at the oxadiazole could form a hydrogen bond with Gly262 (Fig. 4A). On the other hand, we performed a *in silico* docking of **F04** with a TDO protein structure (PDB id: 6A4I) which was released recently (no IDO2 protein structure reported yet). As expected, as shown in Fig. 4C and 4D, compound **F04** was well tolerated in TDO ligand-binding pocket comparing to epacadostat. Additional hydrogen bonds were formed between phosphonamidate moiety and Arg144 with the help of extended side chain which may be responsible for a higher affinity of **F04** toward TDO than

epacadostat. The preliminary docking results may support the fact that the compound **F04** was excellent inhibitor of IDO1 and explain the improved inhibitory activity against TDO.

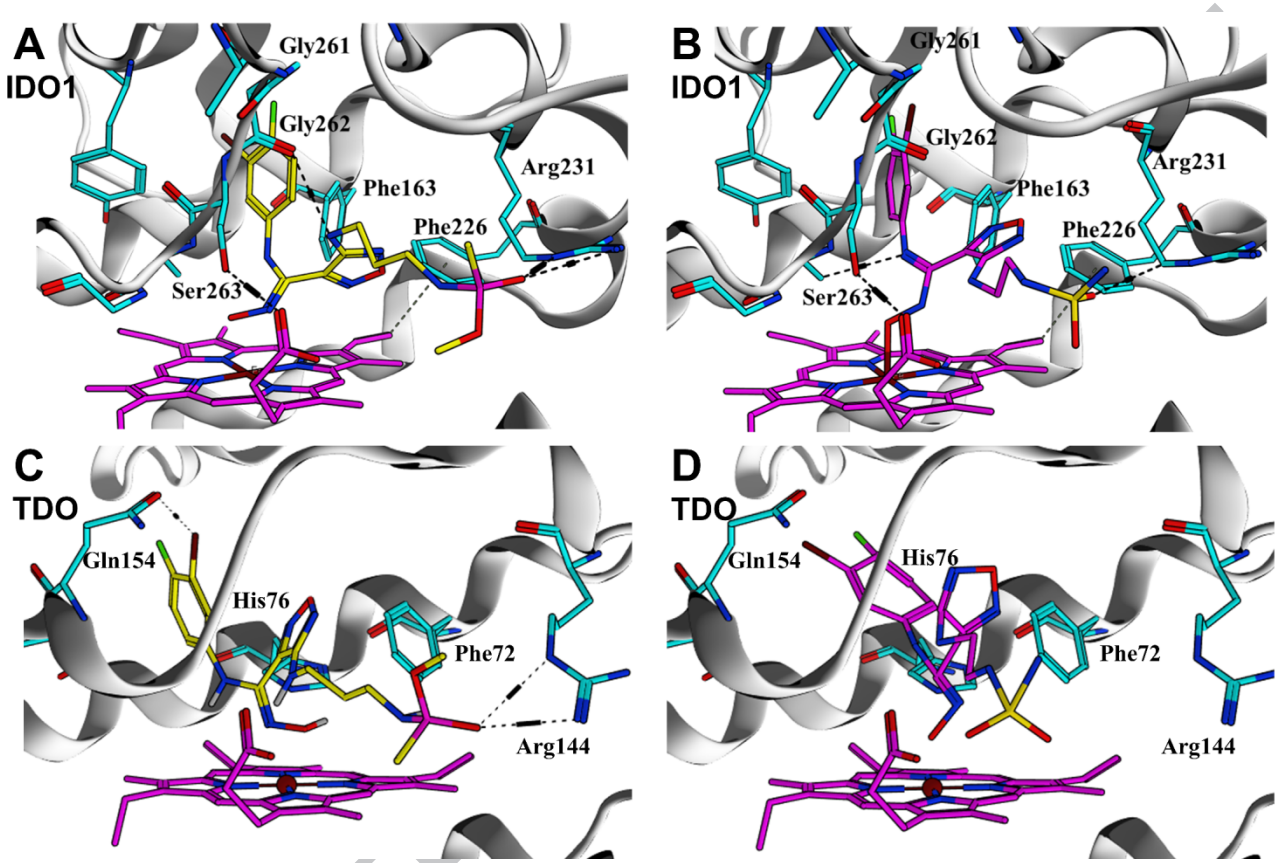

Fig. 4. The docking poses of compound **F04** (A and C, shown in yellow) and epacadostat (B and D, shown in purple) in IDO1 and TDO. The interaction mode was obtained through molecular docking (PDB id:5WN8 for IDO1 and PDB id: 6A4I for TDO) and depicted using MOE 2018.01. The key residues are shown as cyan sticks and H-bonds are shown as black dot lines.

*3.5. **F04** dose-dependently inhibited outgrowth of IDO1-expressing Lewis cells inoculated in immunocompetent C57BL6 mice.*

To investigate whether **F04** could inhibit the outgrowth of transplanted syngeneic tumors *in vivo*, immunocompetent C57BL6 mice were challenged with IDO1-expressing Lewis lung carcinoma cells and treated with different doses (15/30/60 mg/kg) of **F04** or epacadostat (60 mg/kg). **F04** inhibited

tumor volume in a dose-dependent manner through reducing tumor volume by 32%, 50% and 73% at 15, 30 and 60 mg/kg, respectively (Fig. 5A and 5B). Interestingly, positive control epacadostat treatment at 60 mg/kg reduced tumor volume by 68%, displaying a weaker antitumor efficacy as comparing to **F04** (60 mg/kg) (p > 0.05). Similarly, a significant decrease in tumor growth was observed in **F04**- or epacadostat-treated mice comparing to vehicle-treated mice (Fig. 5C). Meanwhile, body weight was markedly increased in mice that received both **F04** (30 mg/kg and 60 mg/kg) and epacadostat treatments comparing to mice received vehicle treatment (Fig. 5D). In the context of these results, treatment with compound **F04** resulted in a significant inhibitory effect on transplanted tumor outgrowth.

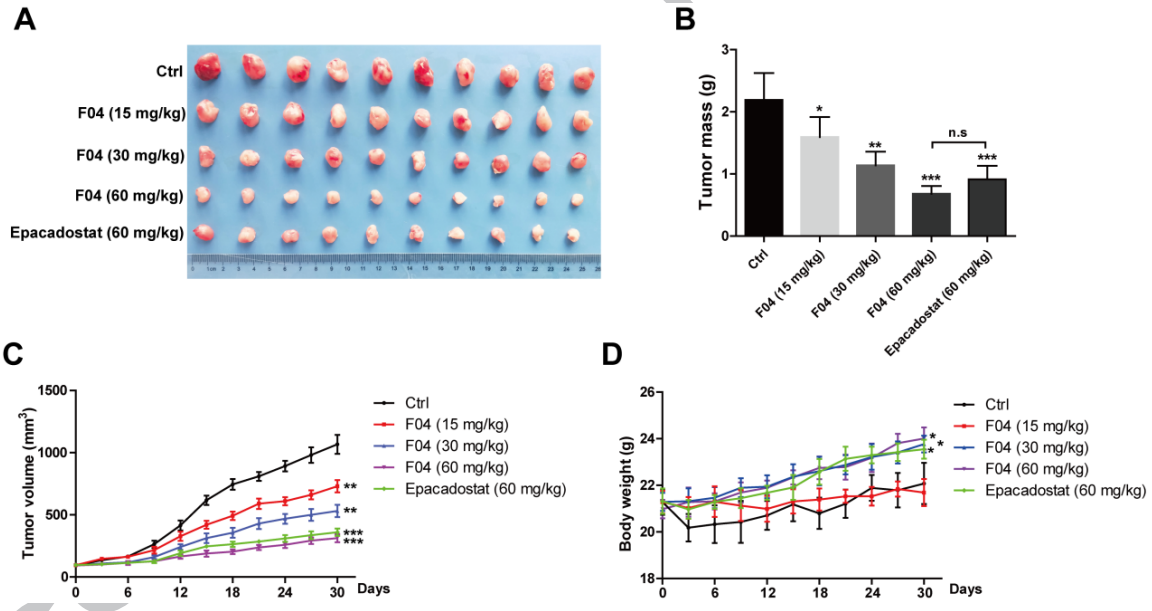

Fig. 5. F04 dose-dependently inhibited outgrowth of IDO1-expressing Lewis cells inoculated in immunocompetent C57BL6 mice. Mice were administered i.g. daily with the indicated compounds following s.c. challenge with 6×10^5 Lewis tumor cells. (A) Representative photograph of excised Lewis tumors (n = 10 for each treatment group). (B) Tumor mass in immunocompetent mice (n = 10 for each treatment group). (C) Tumor growth in immunocompetent mice (n = 10 mice, each. The average tumor volume of Ctrl, **F04** 15/30/60 mg/kg, and epacadostat 60 mg/kg are 1066, 729, 530, 312, and 359 mm^3 respectively). (D) Body weight of immunocompetent mice for each treatment group. Statistical significance was evaluated by one-way ANOVA test (* P <0.05; ** P < 0.01; *** P < 0.001 vs Ctrl group; n.s., not significant).

*3.6. **F04** treatment reduced the Kyn/Trp ratio both in plasmas and tumors.*

As the tryptophan degradation and kynurenine production are indicators of IDO1/TDO/IDO2 activity which can be reflected by the Kyn/Trp ratio, we sought to determine the Kyn/Trp ratio in mice treated with compound **F04**. As shown in Fig. 6A and 6B, the kynurenine/tryptophan ratio in plasmas and tumor tissues were reduced by **F04** treatment in a dose-dependent manner, displaying that **F04** effectively inhibited IDO1/TDO/IDO2 enzyme activity. Importantly, tumors from **F04**-treated mice at 60 mg/kg exhibited a markedly reduced Kyn/Trp ratio comparing to epacadostat ($p < 0.05$).

*3.7. **F04** treatment increased accumulation and infiltration of T cells in transplanted syngeneic tumors.*

Moreover, we observed a significantly increased number of tumor-infiltrating CD8 effector T cells ($CD8^+CD45^+$) in mice treated with **F04** as comparing to mice from Ctrl group (Fig. 6C). The infiltration of proliferative CD8 effector T cells within the transplanted tumors was also increased by **F04** treatment, as measured by the expression of Ki67, a widely used cell proliferating marker (Fig. 6D). By contrast, tumors from **F04**-treated mice displayed a robustly reduced infiltration of regulatory T cells ($CD4^+Foxp3^+CD45^+$) comparing to vehicle-treated mice (Fig. 6E). A dramatic decrease in the percentage of proliferative regulatory T cells was also detected within transplanted tumors in **F04**-treated mice (Fig. 6F). Intratumoral ratios of CD4 effector T cells ($CD4^+Foxp3^-CD45^+$) to regulatory T cells ($CD4^+Foxp3^+CD45^+$) were significantly elevated in **F04**-treated mice as comparing to Ctrl group (Fig. 6G). Additionally, a robustly elevated infiltration of proliferative CD8 effector T cells ($Ki67^+CD8^+$) within transplanted tumors was confirmed with the immunofluorescence analysis in **F04**-treated mice (Fig. 6H). Taken together, these results suggest that **F04** treatment increased the number of accumulation and infiltration of T cells in transplanted tumors and indicated that the pan inhibitor of the Trp catabolizing enzymes may possess more advantage than the selective inhibitor.

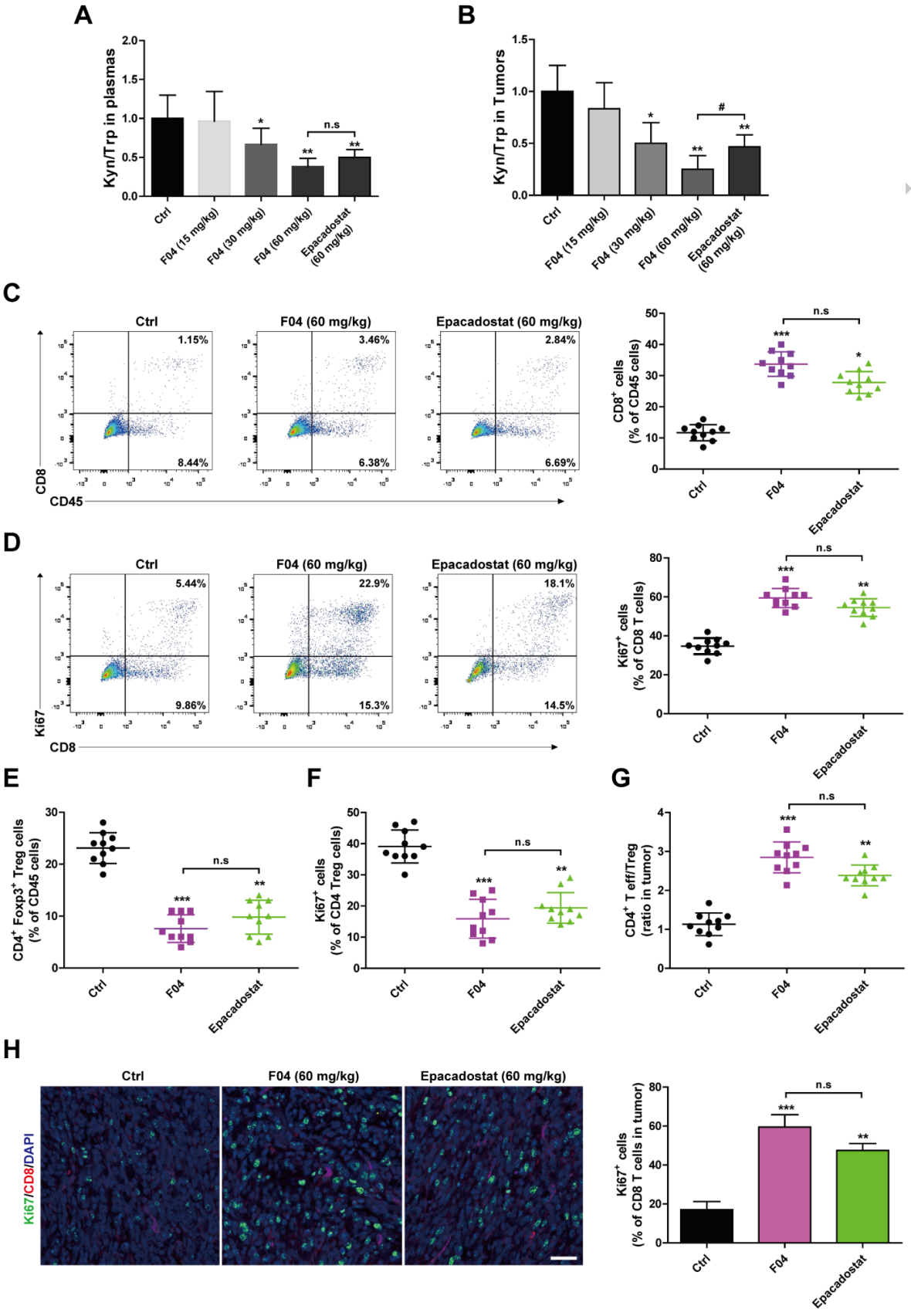
A
Kyn/Trp in plasmas
Ctrl
F04 (15 mg/kg)
F04 (30 mg/kg)
F04 (60 mg/kg)
Epacadostat (60 mg/kg)
n.s
B
Kyn/Trp in Tumors
C
Ctrl
F04 (60 mg/kg)
Epacadostat (60 mg/kg)
1.15%
8.44%
3.46%
6.38%
2.84%
6.69%
CD8
CD45
CD8+ cells (% of CD45 cells)
D
5.44%
9.86%
22.9%
15.3%
18.1%
14.5%
Ki67
Ki67+ cells (% of CD8 T cells)
E
CD4+ Foxp3+ Treg cells (% of CD45 cells)
F
Ki67+ cells (% of CD4 Treg cells)
G
CD4+ T eff/Treg (ratio in tumor)
H
Ki67/CD8/DAPI
Ki67+ cells (% of CD8 T cells in tumor)

Fig. 6. F04 treatment enhances infiltration and accumulation of T cells in transplanted syngeneic tumors. T cells in transplanted tumors from the indicated groups were subjected to FACS analyses. (A) Ratio of tryptophan to kynurenine concentration in plasmas from immunocompetent mice (n = 10). (B) Ratio of tryptophan to kynurenine concentration in transplanted tumors from immunocompetent mice. (C) Percentage of $CD8^+$ effector T cells of total $CD45^+$ cells (n = 10). (D) Percentage of $CD8^+$ effector T cells expressing Ki67 for the indicated mice (n = 10). (E) Percentage of $CD4^+$ $Foxp3^+$ regulatory T cells of total $CD45^+$ cells for the indicated mice (n = 10). (F) Percentage of $CD4^+Foxp3^+$ regulatory T cells expressing Ki67 for the indicated mice (n = 10). (G) Ratio of $CD4^+Foxp3^-$ effector T cells to $CD4^+Foxp3^+$ regulatory T cells in tumors of indicated mice (n = 10). (H) Representative immunofluorescent images (left panels) and percentage of $CD8^+$ T cells expressing Ki67 for tumors of indicated mice (right panel; 1000 ~ 2000 cells were counted in 10 random fields of each slide). Statistical significance was evaluated by One-way ANOVA test (* $P< 0.05$, ** $P < 0.01$ vs Ctrl; n.s., not significant).

*3.8. **F04** dose-dependently suppressed lung metastasis of Lewis cells*

To further evaluate the *in vivo* antitumor activity of compound **F04**, lung metastasis of Lewis cells model was employed. Immunocompetent C57BL6 mice were challenged with Lewis tumor cells via the tail vein and treated with **F04** or epacadostat. A marked increase in body weight was observed in mice treated with **F04** (30 mg/kg and 60 mg/kg) and epacadostat (Fig. 7A). Importantly, both **F04**- and epacadostat-treated mice displayed significantly increased survival relative to vehicle-treated mice (Fig. 7B). As shown in Fig. 7C and 7D, lung metastatic nodules of mice in Ctrl group receiving pneumonectomy was detected, and **F04** suppressed lung metastasis of Lewis tumor cells in a dose-dependent manner. Similarly, H.E. staining suggested that the area of metastases was much smaller in the lungs from **F04**-treated mice comparing to mice from Ctrl group. Interestingly, an average of 12 lung metastatic nodules per mice was observed in **F04** (60 mg/kg) group and 21 was observed in epacadostat group, implying that **F04** exhibited a more potent inhibitory effect on lung metastasis of Lewis cells than epacadostat at the same dose of 60 mg/kg (Fig. 7D).

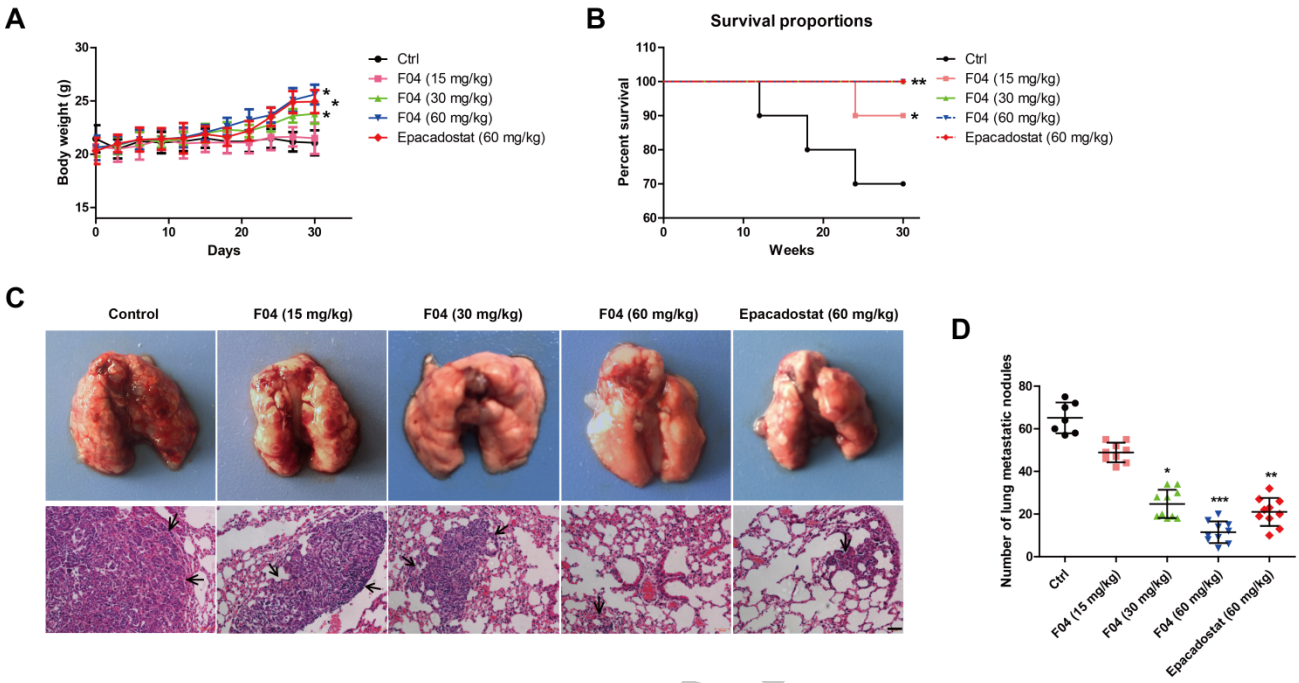

Fig. 7. F04 dose-dependently suppressed lung metastasis of Lewis cells. Lewis tumor cells were injected into the immunocompetent C57BL6 mice via the tail vein. (A) Body weight of immunocompetent mice for each treatment group (on day 30, n = 7 for Ctrl group, n = 9 for **F04**-15 mg/kg, and n = 10 for other groups). (B) Kaplan-Meier survival curves for metastasis tumor-bearing mice. (C) Representative images of lung metastatic nodules in the indicated groups. Arrowheads denote the lung metastatic nodules stained by H&E. Scale bar = 50 μm. (D) The corresponding statistical plots were presented (n = 7 for Ctrl group, n = 9 for **F04**-15 mg/kg, and n = 10 for other groups). Statistical significance was evaluated by One-way ANOVA test (* P< 0.05, ** P < 0.01, *** P < 0.001 vs Ctrl).

4. Discussion

In this work, a novel phosphonamidate derivative **F04** of epacadostat was designed and synthesized. This compound could be considered as bioisostere of sulfonamide-based IDO1 inhibitor. **F04** has been proved to be a pan IDO1/TDO/IDO2 inhibitor targeting Trp/Kyn pathway with potent IDO1 inhibitory activity and moderate potency for IDO2/TDO. Although its inhibitory activity is slightly lower than the best IDO1 inhibitors in the literature, its unexpected pan IDO1/TDO/IDO2 characteristics make lower Kyn/Trp ratio in tumors which was worth for further studying. Indeed, the recent failure of the IDO1-selective inhibitor epacadostat in the ECHO-301 Phase 3 trial in melanoma encouraged the

researchers to orient to discover pan inhibitors targeting Trp/Kyn which may be important to the development of effective therapeutic inhibitors of tryptophan catabolism.

AUTHOR INFORMATION

Corresponding Authors

*E-mail: bianjl@cpu.edu.cn (J. Bian).

*E-mail: zhiyuli@cpu.edu.cn (Z. Li).

Acknowledgements

We gratefully acknowledge financial support from the National Natural Science Foundation of China (no. 81703347, 21672260, and 21372260), the National Natural Science Foundation of Jiangsu Province of China (no. BK20170743 and BK20171393), and the "Double First-class" University Project (CPU2018GY07).

ABBREVIATIONS USED

IDO1, indoleamine 2,3-dioxygenase 1; IDO2, indoleamine 2,3-dioxygenase 1; TDO, tryptophan dioxygenase; $_{L}$-Trp, $_{L}$-tryptophan; KP, kynurenine pathway; NFK, *N*-formylkynurenine; AhR, aryl hydrocarbon receptor; NK, natural killer; Treg, regulatory T cell; MDSC, myeloid-derived suppressor cell; HTS, high-throughput screening; SAR, structure-activity relationship; CDI, *N,N*′-carbonyldiimidazole; rt, room temperature; PSA, polar surface area; HBD, hydrogen bond donor; HBA, hydrogen bond acceptor; LE, ligand efficiency; LLE, lipophilic ligand efficiency; SEM, standard error of the mean; hIFN-*γ*, huaman interferon *γ*; *p*-DMAB, *p*-dimethylaminobenzaldehyde.

REFERENCES

[1] Richard DM, Dawes MA, Mathias CW, Acheson A, Hill-Kapturczak N, Dougherty DM. L-tryptophan: basic metabolic functions, behavioral research and therapeutic indications. *Int. J. Tryptophan Res.* **2009**, *2*, 45–60.

[2] Le Floc'h N, Otten W, Merlot E. Tryptophan metabolism, from nutrition to potential therapeutic applications. *Amino Acids*. **2011**, *41*, 1195–1205.

[3] Routy JP, Routy B, Graziani GM, Mehraj V. The kynurenine pathway is a doubleedged sword in immune-privileged sites and in cancer: implications for immunotherapy. *Int. J. Tryptophan Res.* **2016**, *9*, 67–77.

[4] Weng T, Qiu X, Wang J, Li Z, Bian J. Recent discovery of indoleamine-2,3-dioxygenase 1 inhibitors targeting cancer immunotherapy. *Eur. J. Med. Chem.* **2018**, *143*, 656–669.

[6] Liu M, Wang X, Wang L, Ma X, Gong Z, Zhang S, Li Y. *Hematol. Oncol*. **2018**, *11*, 100.

[6] Munn DH, Mellor AL. Indoleamine 2,3 dioxygenase and metabolic control of immune responses. *Trends Immunol.* **2013**, *34*, 137–143.

[7] van Baren N, Van den Eynde BJ. Tryptophan-degrading enzymes in tumoral immune resistance. *Front. Immunol*. **2015**, *6*, 1–9.

[8] Godin-Ethier J, Hanafi LA, Piccirillo CA, Lapointe R. Indoleamine 2,3-dioxygenase expression in human cancers: clinical and immunologic perspectives. *Clin. Cancer Res*. **2011**, *17*, 6985–6991.

[9] Uyttenhove C, Pilotte L, Theate I, Stroobant V, Colau D, Parmentier N, Boon T, Van den Eynde BJ. Evidence for a tumoral immune resistance mechanism based on tryptophan degradation by indoleamine 2,3-dioxygenase. *Nat. Med*. **2003**, *9*, 1269–1274.

[10] Li A, Barsoumian HB, Schoenhals JE, Cushman TR, Caetano MS, Wang X, Valdecanas DR, Niknam S, Younes AI, Li G, Woodward WA, Cortez MA, Welsh JW. Indoleamine 2,3-dioxygenase 1 inhibition targets anti-PD1-resistant lung tumors by blocking myeloid-derived suppressor cells. *Cancer. Lett*. **2018**, *431*, 54–63.

[11] Holmgaard RB, Zamarin D, Munn DH, Wolchok JD, Allison JP. Indoleamine 2,3-dioxygenase is a critical resistance mechanism in antitumor T cell immunotherapy targeting CTLA-4. *J. Exp. Med*. **2013**, *210*, 1389–1402.

[12] Marin-Acevedo JA, Dholaria B, Soyano AE, Knutson KL, Chumsri S, Lou Y. Next generation of immune checkpoint therapy in cancer: new developments and challenges. *J. Hematol. Oncol*. **2018**, *11*, 39.

[13] Mitchell TC, Hamid O, Smith DC, Bauer TM, Wasser JS, Olszanski AJ, Luke JJ, Balmanoukian AS, Schmidt EV, Zhao Y, Gong X, Maleski J, Leopold L, Gajewski TF. Epacadostat Plus Pembrolizumab in Patients With Advanced Solid Tumors: Phase I Results From a Multicenter,

Open-Label Phase I/II Trial (ECHO-202/KEYNOTE-037). *J. Clin. Oncol.* **2018**, Sep 28: JCO2018789602.

[14] Siu LL, Gelmon K, Chu Q, Pachynski R, Alese O, Basciano P, Walker J, Mitra P, Zhu L, Phillips P, Hunt J, Desai J. Abstract CT116: BMS-986205, an optimized indoleamine 2,3-dioxygenase 1 (IDO1) inhibitor, is well tolerated with potent pharmacodynamic (PD) activity, alone and in combination with nivolumab (nivo) in advanced cancers in a phase 1/2a trial. *Cancer Research*. **2017**, *77*, CT116.

[15] Beatty GL, O'Dwyer PJ, Clark J, Shi JG, Bowman KJ, Scherle PA, Newton RC, Schaub R, Maleski J, Leopold L, Gajewski TF. First-in-human phase I study of the oral inhibitor of indoleamine 2,3-dioxygenase-1 epacadostat (INCB024360) in patients with advanced solid malignancies. *Clin. Cancer Res*. **2017**, *23*, 3269–3276.

[16] Ball HJ, Yuasa HJ, Austin CJ, Weiser S, Hunt NH. Indoleamine 2,3-dioxygenase-2; a new enzyme in the kynurenine pathway. *Int. J. Biochem. Cell Biol*. **2009**, *41*, 467–471.

[17] Ball HJ, Jusof FF, Bakmiwewa SM, Hunt NH, Yuasa HJ. Tryptophan-catabolizing enzymes–party of three. *Front. Immunol*. **2014**, *5*, 485.

[18] Metz R, Smith C, DuHadaway JB, Chandler P, Baban B, Merlo LM, Pigott E, Keough MP, Rust S, Mellor AL, Mandik-Nayak L, Muller AJ, Prendergast GC. IDO2 is critical for IDO1-mediated T-cell regulation and exerts a non-redundant function in inflammation. *Int. Immunol*. **2014**, *26*, 357–367.

[19] Cheong JE, Sun L. Targeting the IDO1/TDO2-KYN-AhR pathway for cancer immunotherapy - challenges and opportunities. *Trends. Pharmacol. Sci*. **2018**, *39*, 307–325.

[20] Muller AJ, Manfredi MG, Zakharia Y, Prendergast GC. Inhibiting IDO pathways to treat cancer: lessons from the ECHO-301 trial and beyond. *Semin. Immunopathol.* **2019**, *41*, 41–48.

[21] Zhou Y, Peng J, Li P, Du H, Li Y, Li Y, Zhang L, Sun W, Liu X, Zuo Z. Discovery of novel indoleamine 2,3-dioxygenase 1 (IDO1) inhibitors by virtual screening. *Comput. Biol. Chem*. **2018**, *78*, 306–316.

[22] Prendergast GC, Malachowski WJ, Mondal A, Scherle P, Muller AJ. Indoleamine 2,3-dioxygenase and its therapeutic inhibition in cancer. *Int. Rev. Cell Mol. Biol*. **2018**, *336*, 175–203.

[23] Winters M, DuHadaway JB, Pham KN, Lewis-Ballester A, Badir S, Wai J, Sheikh E, Yeh SR, Prendergast GC, Muller AJ, Malachowski WP. Diaryl hydroxylamines as pan or dual inhibitors of indoleamine 2,3-dioxygenase-1, indoleamine 2,3-dioxygenase-2 and tryptophan dioxygenase. *Eur. J. Med. Chem*. **2019**, *162*, 455–464.

[24] McAnoy AM, Williams J, Paine MR, Rogers ML, Blanksby SJ. Ion-molecule reactions of O,S-dimethyl methylphosphonothioate: evidence for intramolecular sulfur oxidation during VX perhydrolysis. *J. Org. Chem.* **2009**, *74*, 9319–9327.

[25] Tao M, Frietze W, Meloni DJ, Weng L, Zhou J, Pan Y. Process for the synthesis of an indoleamine 2,3-dioxygenase inhibitor. Patent WO 2015/07007, **2015**.

[26] Feng X, Qiu X, Huang H, Wang J, Xu X, P. Xu, R. Ge, X. Liu, Z. Li, J. Bian, Palladium(II)-catalyzed reaction of lawsones and propargyl carbonates: construction of 2,3-furanonaphthoquinones and evaluation as potential indoleamine 2,3-dioxygenase inhibitors. *J. Org. Chem*. **2018**, *83*, 8003–8010.

[27] Yue EW, Sparks R, Polam P, Modi D, Douty B, Wayland B, Glass B, Takvorian A, Glenn J, Zhu W, Bower M, Liu X, Leffet L, Wang Q, Bowman KJ, Hansbury MJ, Wei M, Li Y, Wynn R, Burn TC, Koblish HK, Fridman JS, Emm T, Scherle PA, Metcalf B, Combs AP. INCB24360 (Epacadostat), a highly potent and selective indoleamine-2,3-dioxygenase 1 (IDO1) inhibitor for immuno-oncology. *ACS. Med. Chem. Lett.* **2017**, *8*, 486–491.

[28] Veber DF, Johnson SR, Cheng HY, Smith BR, Ward KW, Kopple KD. Molecular properties that influence the oral bioavailability of drug candidates. *J. Med. Chem*. 2002, *45*, 2615–2623.

[29] Lipinski CA, Lombardo F, Dominy BW, Feeney PJ. Experimental and computational approaches to estimate solubility and permeability in drug discovery and development settings. *Adv. Drug Delivery Rev*. **1997**, *23*, 3–25.

[30] Hopkins AL, Keseru GM, Leeson PD, Rees DC, Reynolds CH. The role of ligand efficiency metrics in drug discovery. *Nat. Rev. Drug Discov*. **2014**, *13*, 105–121.

[31] Lewis-Ballester A, Pham KN, Batabyal D, Karkashon S, J. Bonanno B, Poulos TL, Yeh SR. Structural insights into substrate and inhibitor binding sites in human indoleamine 2,3-dioxygenase 1. *Nat. Commun*. **2017**, *8*, 1693.

Fig. 1. Structure of candidate epacadostat and the structure of compound **F04** contained in the rectangle with broken line was modified from epacadostat with the phosphonamidate moiety.

Fig. 2. Synthetic scheme for **F04.**

Fig. 3. The inhibitory curves of compound **F04** and epacadostat targeting IDO1-HeLa (A); hIDO1 (B); hIDO2 (C) and TDO (D).

Fig. 4. The docking poses of compound **F04** (A and C, shown in yellow) and epacadostat (B and D, shown in purple) in IDO1 and TDO. The interaction mode was obtained through molecular docking (PDB id:5WN8 for IDO1 and PDB id: 6A4I for TDO) and depicted using MOE 2018.01. The key residues are shown as cyan sticks and H-bonds are shown as black dot lines.

Fig. 5. F04 dose-dependently inhibited outgrowth of IDO1-expressing Lewis cells inoculated in immunocompetent C57BL6 mice. Mice were administered i.g. daily with the indicated compounds following s.c. challenge with 6×10^5 Lewis tumor cells. (A) Representative photograph of excised Lewis tumors (n = 10 for each treatment group). (B) Tumor mass in immunocompetent mice (n = 10 for each treatment group). (C) Tumor growth in immunocompetent mice (n = 10 mice, each. The average tumor volume of Ctrl, **F04** 15/30/60 mg/kg, and epacadostat 60 mg/kg are 1066, 729, 530, 312, and 359 mm^3 respectively). (D) Body weight of immunocompetent mice for each treatment group. Statistical significance was evaluated by one-way ANOVA test (* $P < 0.05$; ** $P < 0.01$; *** $P < 0.001$ vs Ctrl group; n.s., not significant).

Fig. 6. F04 treatment enhances infiltration and accumulation of T cells in transplanted syngeneic tumors. T cells in transplanted tumors from the indicated groups were subjected to FACS analyses. (A) Ratio of tryptophan to kynurenine concentration in plasmas from immunocompetent mice (n = 10). (B) Ratio of tryptophan to kynurenine concentration in transplanted tumors from immunocompetent mice. (C) Percentage of $CD8^+$ effector T cells of total $CD45^+$ cells (n = 10). (D) Percentage of $CD8^+$ effector T cells expressing Ki67 for the indicated mice (n = 10). (E) Percentage of $CD4^+$ $Foxp3^+$ regulatory T cells of total $CD45^+$ cells for the indicated mice (n = 10). (F) Percentage of $CD4^+Foxp3^+$ regulatory T cells expressing Ki67 for the indicated mice (n = 10). (G) Ratio of $CD4^+Foxp3^-$ effector T cells to $CD4^+Foxp3^+$ regulatory T cells in tumors of indicated mice (n = 10). (H) Representative immunofluorescent images (left panels) and percentage of $CD8^+$ T cells expressing Ki67 for tumors of indicated

mice (right panel; 1000 ~ 2000 cells were counted in 10 random fields of each slide). Statistical significance was evaluated by One-way ANOVA test (* P< 0.05, ** P < 0.01 vs Ctrl; n.s., not significant).

Fig. 7. F04 dose-dependently suppressed lung metastasis of Lewis cells. Lewis tumor cells were injected into the immunocompetent C57BL6 mice via the tail vein. (A) Body weight of immunocompetent mice for each treatment group (on day 30, n = 7 for Ctrl group, n = 9 for **F04**-15 mg/kg, and n = 10 for other groups). (B) Kaplan-Meier survival curves for metastasis tumor-bearing mice. (C) Representative images of lung metastatic nodules in the indicated groups. Arrowheads denote the lung metastatic nodules stained by H&E. Scale bar = 50 μm. (D) The corresponding statistical plots were presented (n = 7 for Ctrl group, n = 9 for **F04**-15 mg/kg, and n = 10 for other groups). Statistical significance was evaluated by One-way ANOVA test (* P< 0.05, ** P < 0.01, *** P < 0.001 vs Ctrl).

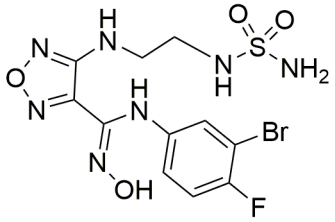

Epacadostat, INCB24360
Incyte, 2012
Phase III Clinical Trials

Phosphonamidate

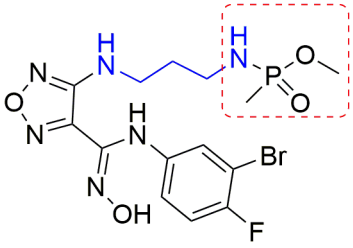

F04

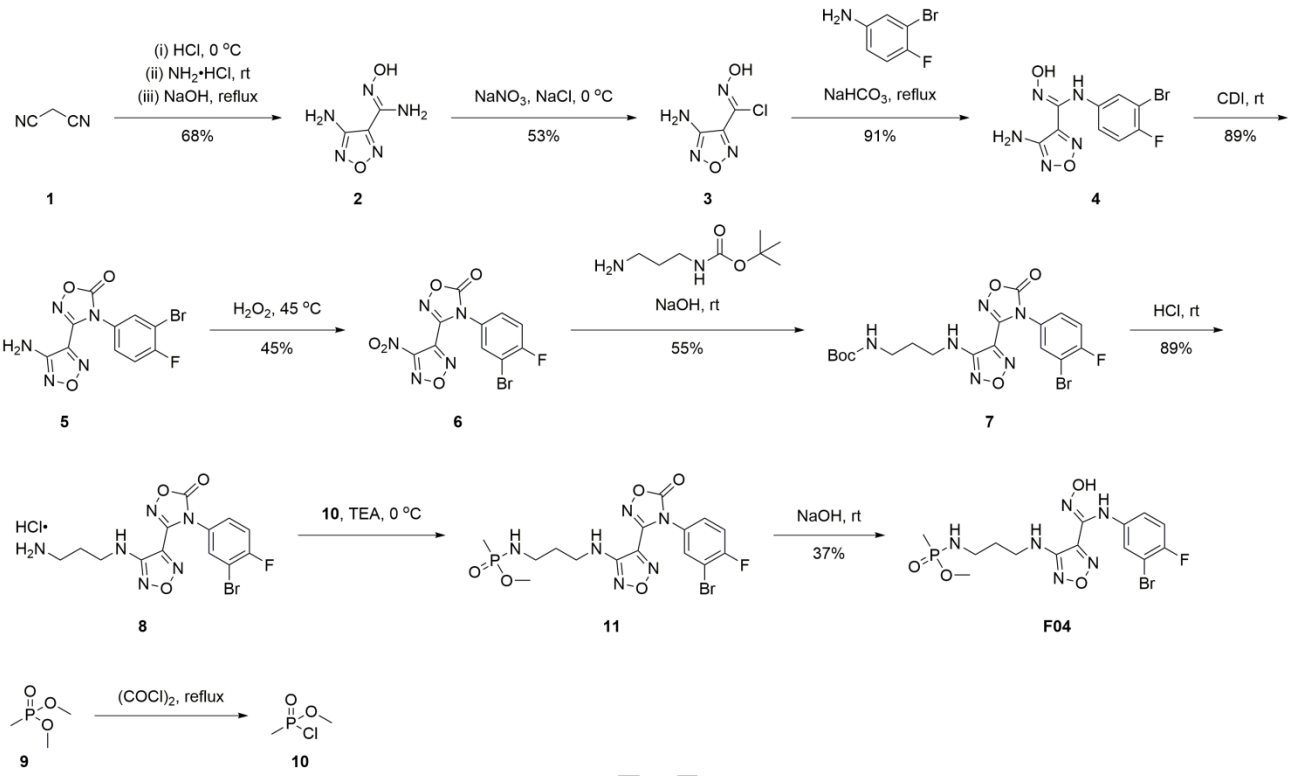
(i) HCl, 0 °C
(ii) NH2•HCl, rt
(iii) NaOH, reflux
68%
NaNO3, NaCl, 0 °C
53%
NaHCO3, reflux
91%
CDI, rt
89%
H2O2, 45 °C
45%
NaOH, rt
55%
HCl, rt
89%
10, TEA, 0 °C
NaOH, rt
37%
(COCl)2, reflux
1
2
3
4
5
6
7
8
11
F04
9
10

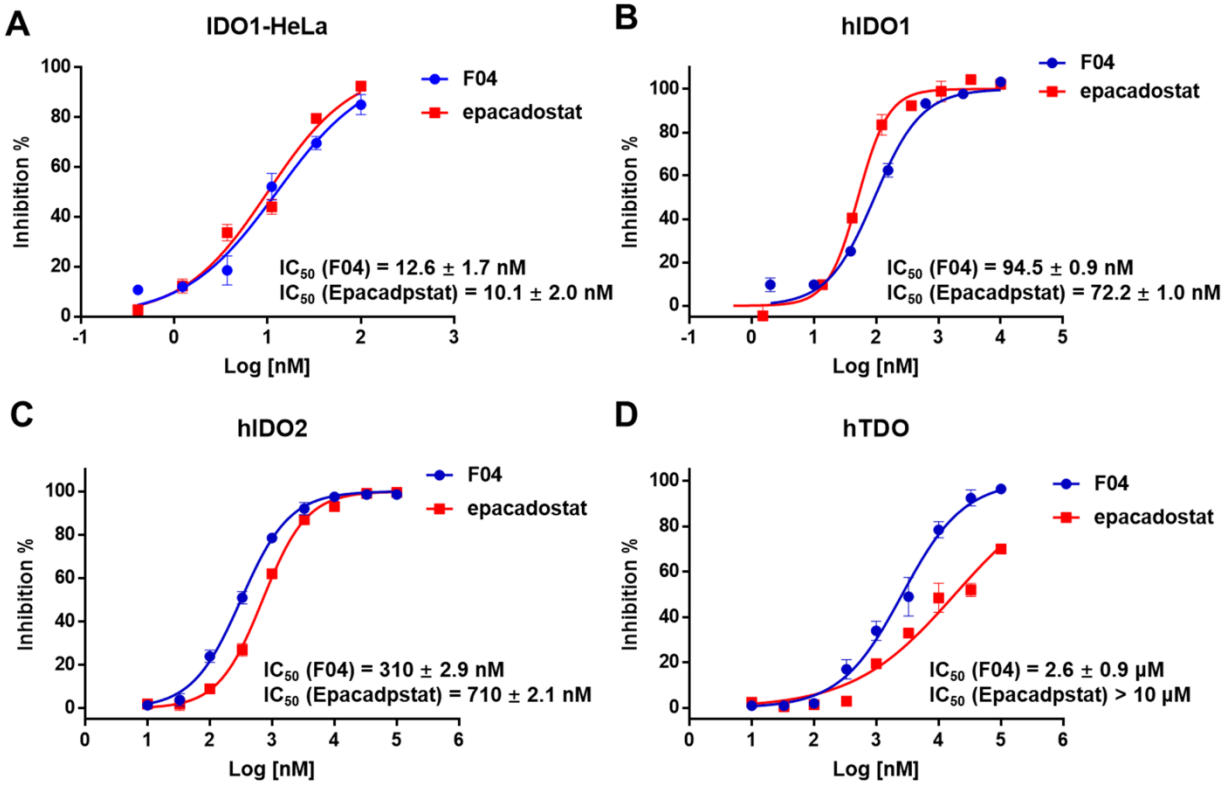
A
IDO1-HeLa
F04
epacadostat
Inhibition %
Log [nM]
IC50 (F04) = 12.6 ± 1.7 nM
IC50 (Epacadpstat) = 10.1 ± 2.0 nM
B
hIDO1
IC50 (F04) = 94.5 ± 0.9 nM
IC50 (Epacadpstat) = 72.2 ± 1.0 nM
C
hIDO2
IC50 (F04) = 310 ± 2.9 nM
IC50 (Epacadpstat) = 710 ± 2.1 nM
D
hTDO
IC50 (F04) = 2.6 ± 0.9 μM
IC50 (Epacadpstat) > 10 μM

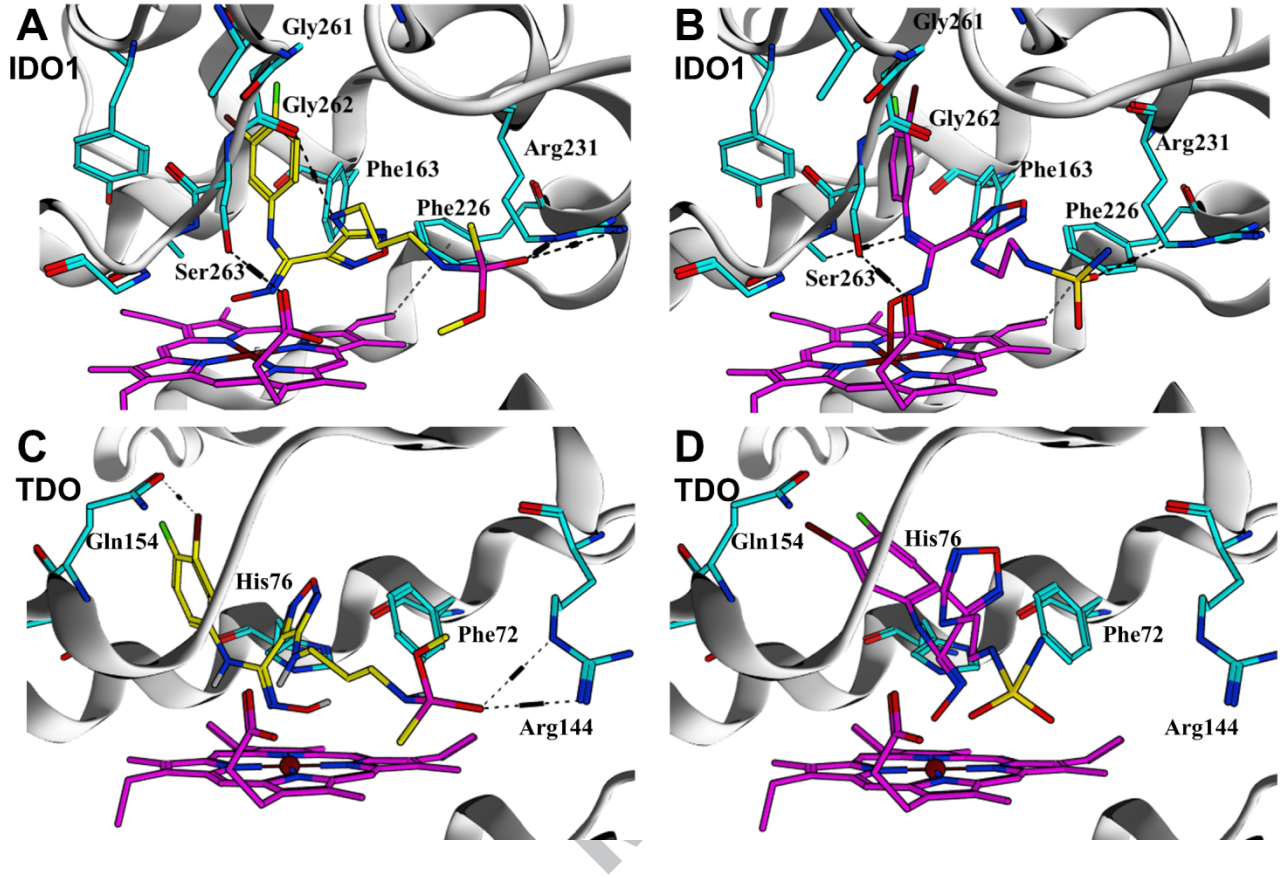
A
IDO1
Gly261
Gly262
Arg231
Phe163
Phe226
Ser263
B
IDO1
Gly261
Gly262
Arg231
Phe163
Phe226
Ser263
C
TDO
Gln154
His76
Phe72
Arg144
D
TDO
Gln154
His76
Phe72
Arg144

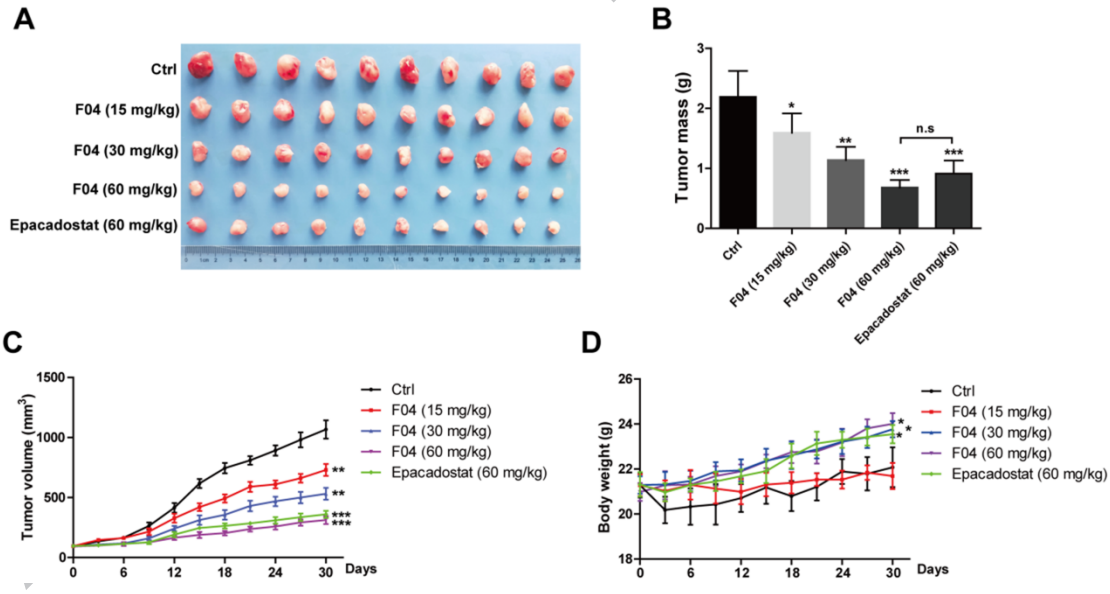
A
Ctrl
F04 (15 mg/kg)
F04 (30 mg/kg)
F04 (60 mg/kg)
Epacadostat (60 mg/kg)
B
Tumor mass (g)
n.s
Ctrl
F04 (15 mg/kg)
F04 (30 mg/kg)
F04 (60 mg/kg)
Epacadostat (60 mg/kg)
C
Tumor volume (mm3)
Days
Ctrl
F04 (15 mg/kg)
F04 (30 mg/kg)
F04 (60 mg/kg)
Epacadostat (60 mg/kg)
D
Body weight (g)
Days
Ctrl
F04 (15 mg/kg)
F04 (30 mg/kg)
F04 (60 mg/kg)
Epacadostat (60 mg/kg)

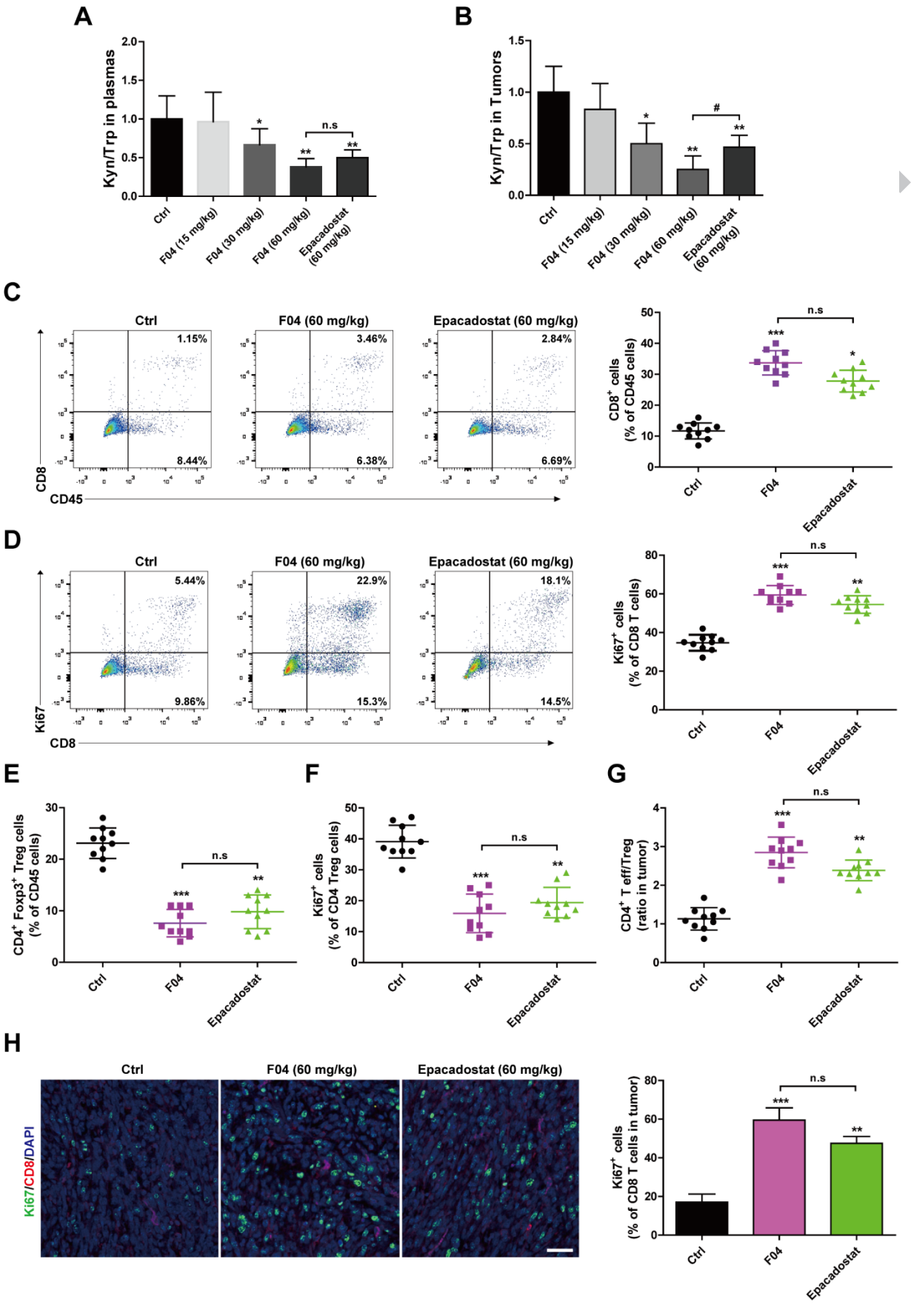
A
Kyn/Trp in plasmas
Ctrl
F04 (15 mg/kg)
F04 (30 mg/kg)
F04 (60 mg/kg)
Epacadostat (60 mg/kg)
n.s
B
Kyn/Trp in Tumors
C
Ctrl
F04 (60 mg/kg)
Epacadostat (60 mg/kg)
1.15%
8.44%
3.46%
6.38%
2.84%
6.69%
CD8
CD45
CD8+ cells (% of CD45 cells)
F04
Epacadostat
D
5.44%
9.86%
22.9%
15.3%
18.1%
14.5%
Ki67
Ki67+ cells (% of CD8 T cells)
E
CD4+ Foxp3+ Treg cells (% of CD45 cells)
F
Ki67+ cells (% of CD4 Treg cells)
G
CD4+ T eff/Treg (ratio in tumor)
H
Ki67/CD8/DAPI
Ki67+ cells (% of CD8 T cells in tumor)